Split-enabled 350-630 Gb/s Optical Interconnect with Direct Detection NOMA-CAP and 7-Core Multi-Core Fiber

Samael Sarmiento[1, 2,*], José Manuel Delgado Mendinueta[2], José Antonio Altabás[3,4], Salvatore Spadaro[1], Satoshi Shinada[2], Hideaki Furukawa[2], Juan José Vegas Olmos[5], José Antonio Lázaro[1], Naoya Wada[2]

[1]School of Telecommunications Engineering, Polytechnic University of Catalonia, Barcelona 08034, Spain
[2]Photonic Network System Laboratory, National Institute of Information and Communication Technology (NICT), 4-2-1 Nukui-Kitamachi, Koganei, Tokyo 184-8795, Japan
[3]Bifrost Communications, Scion DTU, Akademivej Bygnig 381, 2800 Kgs Lyngby, Denmark
[4]Aragon Institute of Engineering Research, University of Zaragoza, Zaragoza 50018, Spain
[5]Mellanox Technologies, Yokneam, 20692, Israel
*Corresponding author: samael.sarmiento@tsc.upc.edu

Abstract: The ever-growing data traffic volume inside data centers caused by the popularization of cloud services and edge computing demands scalable and cost-efficient network infrastructures. With this premise, optical interconnects have recently gained more and more research attention as a key building block to ensure end-to-end energy efficient solutions, offering high throughput, low latency and reduced energy consumption compared to current networks based on active optical cables. An efficient way for performing such optical interconnects is to make use of multi-core fibers (MCFs), which enables the multiplexing of several spatial channels, each using a different core inside the same fiber cladding. Moreover, non-orthogonal multiple access combined with multi-band carrierless amplitude and phase modulation (NOMA-CAP) has been recently proposed as a potential candidate to increase the network capacity and an efficiency/flexibility resource management. In this paper, using direct detection we experimentally demonstrate the transmission of NOMA-CAP signals through a 2 km MCF with 7 spatial channels for high capacity optical interconnect applications. The results show negligible transmission penalty for different total aggregated traffics ranging from 350 Gb/s to 630 Gb/s.

1. INTRODUCTION

The requirements on interconnect capacity for data center applications continue to steadily grow and there is a reasonable concern on whether four-level pulse amplitude modulation (PAM-4) can scale beyond 100 Gb/s per lane [1]. On the electrical domain, integrated circuits may go to smaller manufacturing processes, from the current 22 nm to 7 nm [2, 3]. However, the reduction in power consumption may not scale linearly with the process shrinking and costs may become prohibitive. The electrical bandwidth requirement for 200 Gb/s PAM-4 would be near 80-100 GHz, and silicon photonics, indium phosphide or heterogeneous integration are promising technologies but not yet mature enough to have significant yield

with this specification in volume production [4]. There is therefore a need to exploit and investigate alternative dimensions and/or modulation formats to increase the capacity of optical interconnects.

Currently, there is momentum for coherent technologies to penetrate the short-range segment in data centers (<2 km), although costs remain a huge challenge given the complexity of the optical layer, the power consumption, the digital signal processing (DSP) complexity and the increased latency. Alternatively, faster-than-Nyquist (FTN) signaling is a promising solution to increase the symbol rate of intensity-modulation/direct-detection (IM/DD) systems. However, working in C band, transmitting at symbol rates beyond the Nyquist rate is challenging due to the spectral power fading caused by the chromatic dispersion (CD). To overcome that limitation, maximum likelihood sequence estimation (MLSE) [5-10] and Tomlinson-Harashima precoding (THP) [11-13] techniques along with feed-forward equalization (FFE) have recently been proposed for PAM signals, achieving bit rates around 200 Gb/s per lane with 33 GHz electrical bandwidth devices.

More advanced modulations formats such as discrete-multitone (DMT) and multi-band carrierless amplitude and phase (multi-CAP) modulation have also been investigated to enhance the CD tolerance of IM/DD systems inside data centers, while increasing the efficiency/flexibility resource management, the optical signal-to-noise ratio (OSNR) performance and the thermal noise tolerance compared to PAM signals at the cost of increasing the DSP complexity [14, 15]. Recently, the transmission of IM-DD DTM and multi-CAP achieving up to 140 Gb/s per lane with 10-20 GHz electrical bandwidth devices and without the use of sophisticated equalization techniques has been demonstrated in [16-19]. In particular, DTM (multi-CAP) enables to load information in selective subcarriers (bands) to avoid the performance degradation around spectral power fades. Although both DTM and multi-CAP systems can offer similar OSNR performance [20], multi-CAP allows for less complex transceivers implementation since no mixers are required [17, 20]. Moreover, multi-CAP shows lower peak-to-average power ratio (PAPR) compared to DTM. Basically, CAP modulation is a multilevel and multidimensional modulation scheme in which data is transmitted through two orthogonal signals. In this scheme, pulse shaping filters are used to generate the two signals and form the time-domain orthogonality [21]. One of the most attractive features of CAP is that the shaping filters can be implemented analogically [17], reducing significatively the DSP complexity of multi-CAP for mid/high number of bands [22].

On the other hand, exploiting spatial diversity through multi-core fibers (MCFs) enables the parallel multiplexing of several spatial channels, while facilitating the assembly process between fiber and the photonic integrated circuits (PICs), most likely through constellations of vertical gratings tapping light in and out of the PIC [23], with a reasonable cost impact. Furthermore, link splitters are becoming more relevant when designing the topology of the network in data center environments as shown in Fig. 1. Split-cable or H-cables allow a system unit with a connector on one side and two or more separate connectors on the other side, such as a spine switch and two or more leaf switches in fabric infrastructures, thereby allowing network topologies relevant for hyperscalers [24, 25]. This feature is particularly interesting in large configurations of high-performance clusters (HPC) within data centers, as the number of layers of switches is reduced and frees up switching ports. Few-mode fibers can also be considered to provide short-range connectivity inside data centers; however, their bandwidth and interconnect span are more restricted than in MCFs [26].

MCF-based IM/DD systems providing 100-150 Gb/s per lane and core have recently been investigated for HPC applications in data centers. In [27], the performance of 150 Gb/s PAM-4, requiring 32 GHz electrical bandwidth, has been demonstrated over 1 km 7-core MCF, achieving the 7% overhead (OH) hard-decision forward error correction (HD-FEC) limit (BER<3.8E-4) for received optical powers higher than 3.0 dBm. 100 Gb/s electrical duobinary (EDB) and 112 Gb/s PAM-4 have also been reported over 1 km 7-core MFC in [28] and [29], respectively. In [28], the 100 Gb/s EDB signal, requiring 15 GHz electrical bandwidth, is generated using a monolithically integrated distributed feedback laser with traveling-wave electroabsorption modulator (DFB-TWEAM), reaching the 7% OH HD-FEC limit for received optical powers higher than 0 dBm. In [29], the 112 Gb/s PAM-4 signal is generated with a 20 GHz 3 dB bandwidth vertical cavity surface emitting laser (VCSEL). In this case, not all cores provide the demanded 7% OH HD-FEC, requiring therefore digital pre- and post-equalization. The 7% OH HD-FEC is then reached for received optical powers higher than 2 dBm. The transmission over 10 km 7-core MCF has also been demonstrated in [27-29] with the use of an optical dispersion compensation module [30] for inter-data center applications.

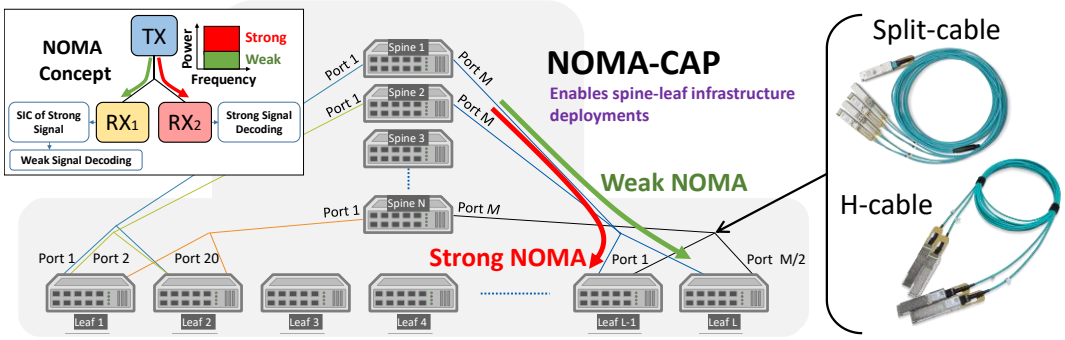

Fig. 1. Architecture of a highly scalable spine-leaf data centre architecture enhanced by split-cables or H-cables. (Inset) NOMA concept.

Non-orthogonal multiple access (NOMA) technique has been proposed to boost further the flexibility of the network [31]. Fig. 1 shows the NOMA concept. NOMA enables a single transmitter to simultaneously transmit two or more different signals using the same wavelength and polarization through power multiplexing, and to recover them through affordable direct detection (DD) [32]. Successive interference cancellation (SIC) is required to retrieve the tributary signals and demultiplex each NOMA signal at the receivers' side [31]. This increases the receiver complexity. To mitigate this issue, redundancy can be added to the signals through spectrum spreading or coding techniques since it facilitates the signals separation, but decreasing the spectral efficiency [33]. Alternatively, SIC can be implemented with moderate complexity, without the need for spreading/coding redundancy, by limiting the number of power multiplexed signals to two and the constellation alphabet to four symbols, as demonstrated in [34]. Moreover, SIC with moderate complexity can be implemented using available technology with a tolerable increase of the energy consumption [35].

The combination of NOMA and multi-CAP (NOMA-CAP) has been experimentally demonstrated in optical access communications such as radio-over-fiber-based fronthauls [32] and passive optical networks (PONs) [36, 37]. Recently, NOMA-CAP and MCF have been experimentally demonstrated for high capacity optical interconnects, supporting a total

aggregated traffic of 490 Gb/s [38]. In this paper, we experimentally demonstrate the transmission of NOMA-CAP through 2 km 7-core MCF using DD and providing different total aggregated traffics ranging from 350 Gb/s to 630 Gb/s, hence increasing the maximum total aggregated traffic of the system by 30% (140 Gb/s) compared to [38]. Specifically, a maximum bit rate of 90 Gb/s, requiring a 3 dB electrical bandwidth of 20 GHz, per lane and core is demonstrated. The 7% OH HD-FEC is achieved without the use of complex equalization techniques for received optical powers higher than -4.2 dBm.

The remainder of this paper is structured as follows. Section 2 describes the implemented optical MCF-based transmission setup as well as the required DSP for the generation and detection of the NOMA-CAP signals when two power levels and different number of 2.5 GHz bands are considered. Section 3 shows the measured experimental results of the system transmission characterization, in back-to-back and through the MCF for different total aggregated traffics. Finally, Section 4 concludes the paper and draws the main conclusions.

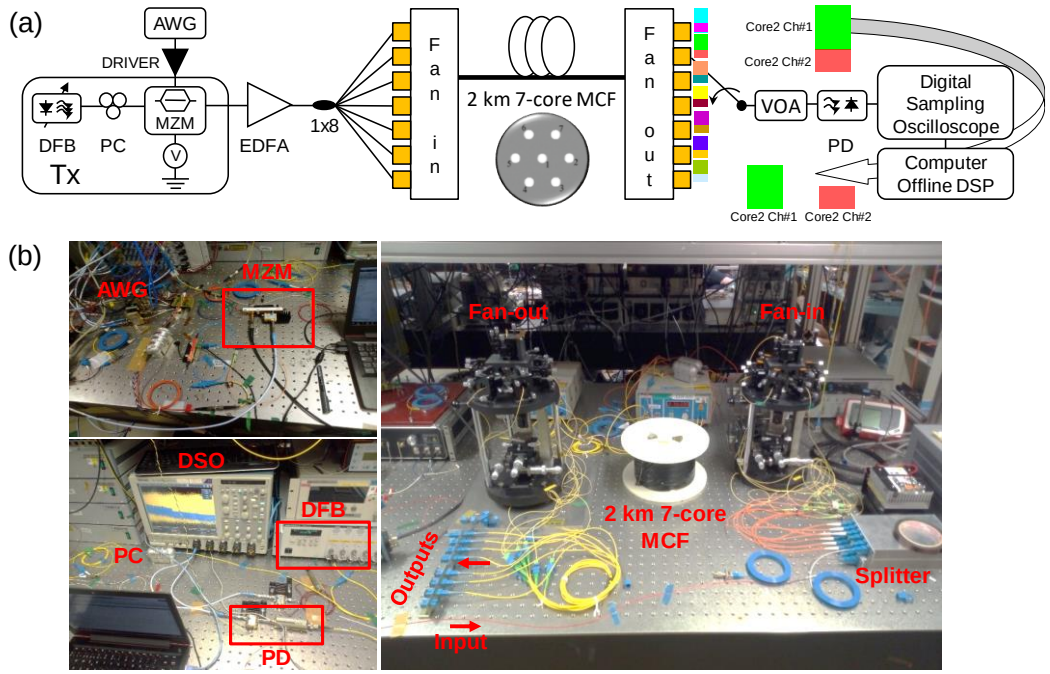

Fig. 2. (a) Schematic of the experimental setup for the NOMA-CAP transmission. (Inset) Microphotography of the 2 km 7-core MCF fiber used in this demonstration. (b) Laboratory setup. (Acronyms) DFB: distributed feedback laser, PC: polarization controller, V: voltage source, AWG: arbitrary waveform generator, EDFA: erbium doped fiber amplifier, MCF: multi-core fiber, VOA: variable optical attenuator, PD: photodiode, DSO: digital sample oscilloscope.

2. EXPERIMENTAL SETUP AND DIGITAL SIGNAL PROCESSING DESCRIPTION

A. MCF-based optical interconnect experimental setup

The experimental setup is shown in Fig. 2. The transmitter used a distributed feedback laser (DFB) set at 1548 nm as a light source which was fed to a Mach-Zehnder modulator (MZM). The optical bandwidth of the MZM was 30 GHz. This transmitter can be integrated through heterogeneous integration, in high-performing indium phosphide, or most likely, through a silicon photonic PIC containing the modulators and arrays of flip-chip DFB lasers [39, 40]. The bias of the MZM was manually set by a voltage source. The MZM was driven with an arbitrary waveform generator (AWG) with 20 GHz 3 dB electrical bandwidth, which

generated the NOMA-CAP modulation, and amplified with a linear electrical driver with 50 GHz of bandwidth. After the MZM, an erbium-doped fiber amplifier (EDFA) was used to amplify the signal and compensate for the losses of the 1x8 splitter, used to simulate traffic coming from 7 different transmitters, each containing two independent data streams as will be explained in the next subsection. The patch-cord lengths of each path were different, hence effectively decorrelating the channels. The seven information-bearing signals were connected to a fan-in device [41], used to multiplex the signals into a 2 km trench-assisted 7-core MCF span. The average attenuation per core was less than 0.2 dB/km at the working wavelength and the average crosstalk after 2 km was of -56.5 dB. After transmission, the signals were demultiplexed using a fan-out device [41]. The receiver consisted of a standard PIN photodiode with an optical bandwidth of 33 GHz followed by a digital sampling oscilloscope (DSO), which was connected manually to each core of the MCF under measurement. The signal was digitized at 100 GS/s although in a real-system 40-45 GS/s would be sufficient to cover the NOMA-CAP signal bandwidth [17]. In this work only one receiver was considered for simplicity, but the different power multiplexed signals can be detected for different receivers as shown in Fig. 1.

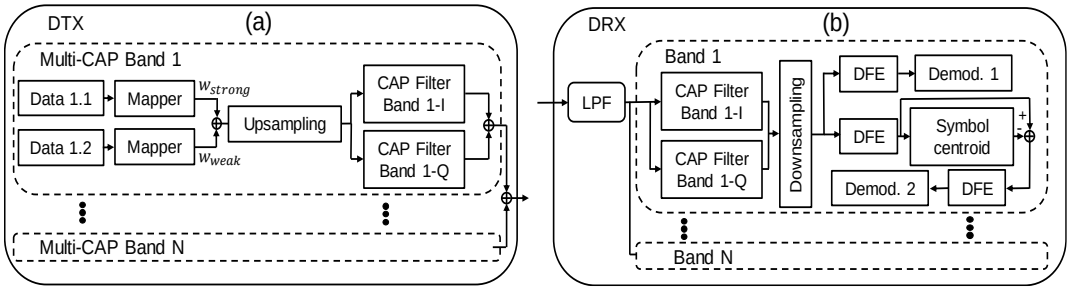

Fig. 3. NOMA-CAP DSP block diagram for: (a) the digital transmitter (DTX) and (b) digital receiver (DRX).

B. Transmitter and receiver DSP architecture

The transmitter DSP architecture for NOMA-CAP transmission with two NOMA levels per band is shown in Fig. 3(a). First, the data of both NOMA levels were distributed among all the multi-CAP bands and mapped into 4-QAM symbols using Gray coding. The two NOMA levels, tagged as "weak NOMA" and "strong NOMA" in this work, were power weighted according to the power ratio r_p, defined as the relation between the two NOMA levels, $r_p = 20\log\left(w_{strong}/w_{\mathrm{weak}}\right)$, and added for each multi-CAP band. The NOMA signal of each multi-CAP band was upsampled to the ratio between the sampling frequency and the symbol rate. The symbol rate was set at 2.5 GBd to provide a total bit rate of 10 Gb/s per band. After the upsampling process, the resulting complex NOMA signals were split into real and imaginary parts and filtered with a pair of band-specific multi-CAP orthogonal filters (h_{I_i} and h_{Q_i}) defined, in time domain, in Eq. (1) and Eq. (2), where $p(t)$ and f_{c_i} are the pulse shaper and the frequency carrier of the multi-CAP band i. Note that the filters h_{I_i} and h_{Q_i} form a Hilbert pair. To improve the spectral efficiency, a square-root raised cosine (SRRC) filter with a roll off factor equal to 0.1 and a length of 20 symbols was employed as $p(t)$ [32, 42]. Therefore, the filtering of each multi-CAP band with the matched filters at the reception side allows extracting the signal and simultaneously minimizing the inter-symbol interference (ISI). Finally, the multi-CAP bands were aggregated to form the complete

transmitted data signal. The number of multi-CAP bands and spectral width can be optimized to maximize the capacity of the link, as it has been done with DTM [43-47]. However, for simplicity in this work two NOMA levels with varying numbers of 2.5 GHz multi-CAP bands, N_{bands}= {5, 7, 9}, were assessed. Fig. 4 shows the impulse response of all considered multi-CAP band filters as well as an example of a NOMA-CAP signal to be transmitted in the time domain.

$$h_{I_i} = p(t)\cos\left(2\pi f_{c_i}\right) \quad (1)$$

$$h_{Q_i} = p(t)\sin\left(2\pi f_{c_i}\right) \quad (2)$$

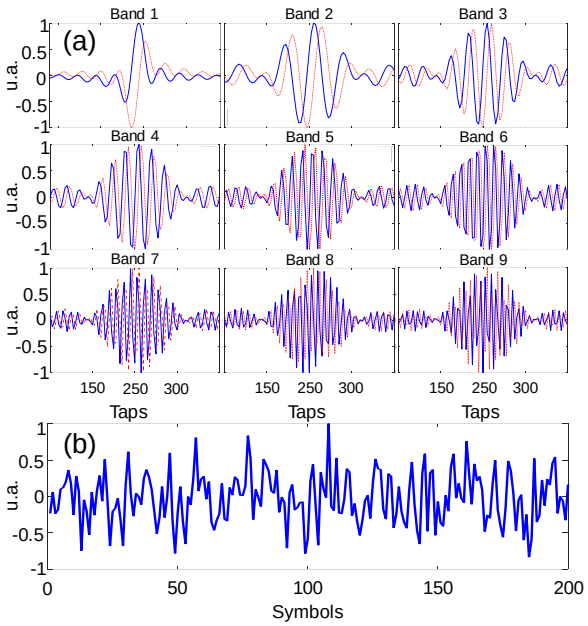

Fig. 4. (a) Temporal response of considered nine multi-CAP band filters (blue line is the I-component and red dotted line is the Q-component). (b) Example of transmitted NOMA-CAP signal in time domain.

The receiver DSP block diagram is shown in Fig. 3(b). As a first step, a low-pass filter of the digitalized signal was performed, to reduce the noise out of band. As second step, a pair of inverted multi-CAP orthogonal filters were used to extract each band of interest. As third step, the strong NOMA level was obtained directly, while for the weak NOMA level, it was implemented a SIC, Fig. 3(b) [31]. It consisted of a decision feedback equalizer (DFE) with 30 forward and 20 backward taps. The SIC then calculated the symbol centroid of the strong NOMA level and subtracts it from the equalized signal. As fourth step, the DFE was applied again, and finally the resulting signal was de-mapped. In case of the strong NOMA level, the de-mapping was performed just after applying the DFE filter, both processes using the same parameters as for the weak NOMA level. For both weak and strong NOMA levels, the phase recovery was performed through training symbols [48, 49], although differential QAM encoding/decoding plus multi-modulus algorithm (MMA)-based equalization can also be used to reduce the spectral efficiency loss due to the training [50, 51].

3. Experimental results and discussion

The back-to-back (B2B) power spectral density of the NOMA-CAP signals is shown in Fig. 5. The NOMA-CAP signal is form out of, respectively: five, seven and nine 2.5 GHz CAP bands.

Thus, providing corresponding bit rates of (R_b): 50 Gb/s, 70 Gb/s and 90 Gb/s. Then requiring electrical bandwidths circa: 14 GHz, 20 GHz and 25 GHz. Thanks to the two NOMA levels per band, the spectral efficiency is close 3.5 b/(s·Hz). Therefore, through the combination of multi-CAP and NOMA techniques, the total data rate and the spectral efficiency is increased.

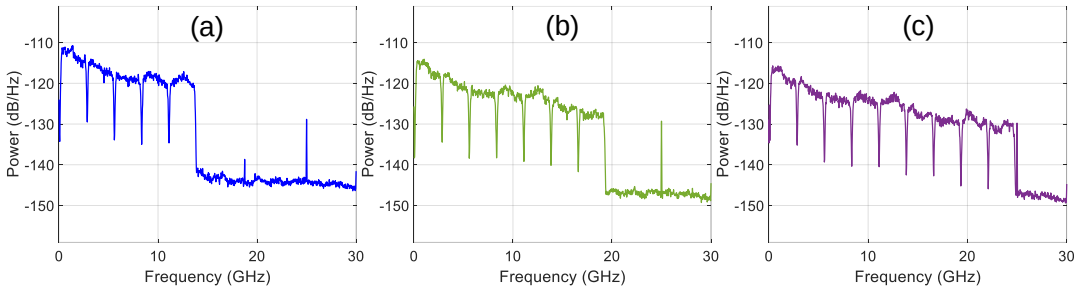

Fig. 5. Power spectral density of NOMA-CAP signal in back-to-back configuration for: (a) 5 CAP bands, (b) 7 CAP bands and (c) 9 CAP bands, providing an aggregated bit rate of 50 Gb/s, 70 Gb/s, and 90 Gb/s, respectively.

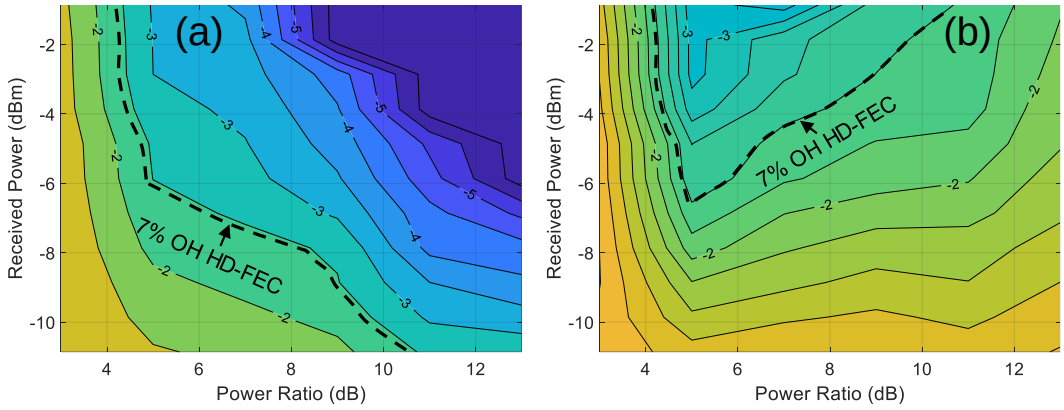

Fig. 6. Contour $\log_{10}$(BER) vs. received power vs. power ratio plots for (a) strong NOMA and (b) weak NOMA levels in back-to-back configuration (no EDFA, no 7-core MCF, ref. Fig. 2) when the number of multi-CAP bands is equal to 7, providing an aggregated bit rate of 70 Gb/s.

The Fig. 6 shows the measured NOMA-CAP system performance for the strong and weak NOMA levels, for the configuration of R_b= 70 Gb/s, i.e., N_{bands}= 7 and in B2B. The bit-error rate (BER) is measured vs. r_p, vs. the received optical power (P_{RX}), and the average value for the 7 bands is shown in Fig. 6. In case of the strong NOMA level, the multiplexed weak NOMA level signal can be seen as an extra noise or interference. Due to that, a reduced r_p value causes a BER degradation decreasing the receiver sensitivity. The receiver sensitivity has been defined as the minimal P_{RX} to achieve a BER=3.8E-3, corresponding to the 7% OH HD-FEC limit. Therefore, higher r_p values are the best scenario for the strong NOMA level since the effect of the weak NOMA level signal on the strong level signal is reduced. For the weak NOMA level, the SIC cancellation must be performed in advance to remove the strong NOMA level signal. Of course, any error in the calculation of the strong NOMA level signal will affect the decoding of the weak NOMA level, causing errors at detection. On the one hand, reducing the P_{RX} increases the number of errors in the centroid calculation, causing a degradation of the BER of the weak NOMA level signal, as can be observed in Fig. 6(b). The use of lower r_p values has a similar effect as reducing P_{RX}. On the other hand, the BER of the weak NOMA level is also degraded with higher r_p values, even if the SIC process perfectly

calculates the strong NOMA level centroids. This is just because higher r_p values mean less weak NOMA level signal at the same P_{RX}. Accordingly, the weak NOMA level can be successfully demodulated only for high P_{RX} values and intermediate r_p values, Fig. 6(b). Though the results are shown for 7 bands, similar behavior was obtained in the case of N_{bands}= {5, 9}. A value r_p= 7 dB has been stablished as a good trade-off, optimizing the receiver sensitivity for both NOMA levels and all the considered aggregated bit rates.

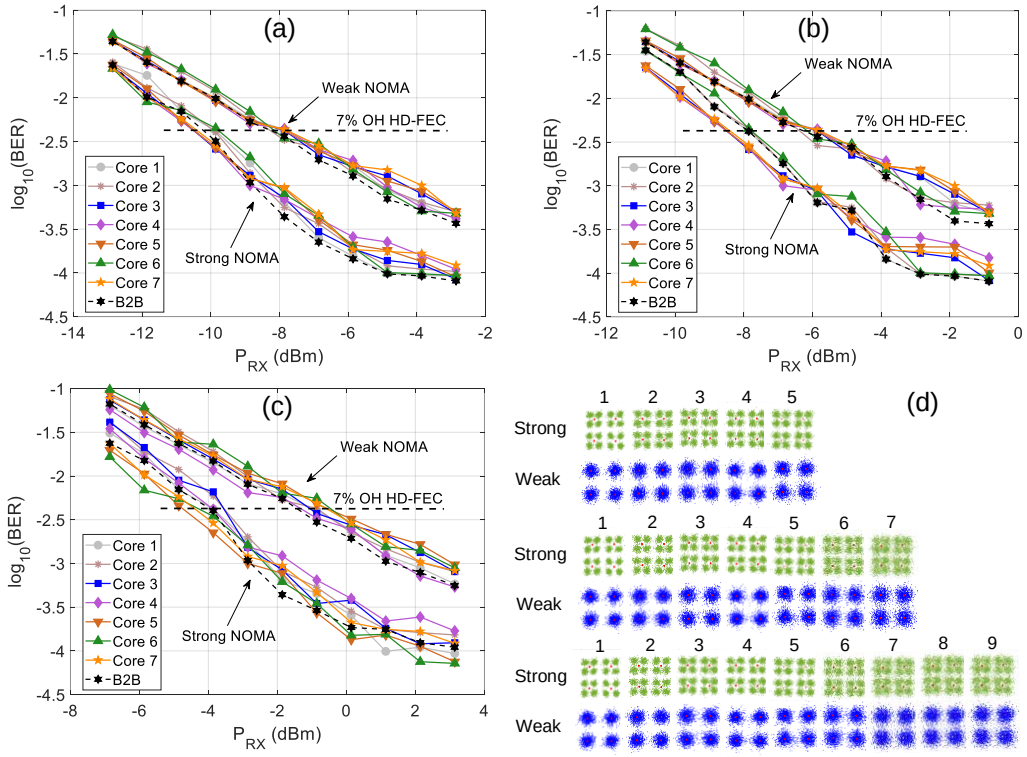

Fig. 7. BER vs. received power (P_{RX}) of the weak and strong NOMA levels when the NOMA-CAP signal is transmitted in back-to-back (B2B) configuration and through the 2 km MCF with 7 cores for a total aggregated bit rate per lane of: (a) 50 Gb/s, (b) 70 Gb/s and (c) 90 Gb/s, providing a total aggregated traffic of 350 Gb/s, 490 Gb/s and 690 Gb/s, respectively. (d) Received constellations at the FEC limit for B2B configuration of the strong and weak NOMA levels for N_{bands}= {5, 7, 9}. Red circles are the constellation centroids.

Fig. 7(a-c) shows the measured averaged BER vs. P_{RX} curves of the weak and strong NOMA levels when the NOMA-CAP signal is transmitted in B2B configuration for R_b= {50, 70, 90} Gb/s, corresponding to N_{bands}= {5, 7, 9}, respectively. For each considered R_b value, Fig. 7(d) shows the received constellations on each band and each NOMA level at the considered FEC limit. Table 1 summarizes the B2B receiver sensitivities depicted in Fig. 7(a-c) as well as the BER of each band and each NOMA level at the FEC limit of 7% OH HD-FEC. As it can be seen, the sensitivity penalty for weak and strong NOMA levels increases by 2.0 dB when the bit rate upgrades from 50 Gb/s to 70 Gb/s. While the sensitivity penalty reaches 7.5 dB for a more ambitious bit rate upgrade from 50 Gb/s to 90 Gb/s. This is due to the electrical bandwidth limitation at the transmitter and receiver sides as it can be seen in Fig. 5, at the power spectral densities. Form Table 1, it can also be observed that the BER of each multi-CAP band is lower than 7.8E-4, BER value corresponding a maximum penalty of 1 dB over the receiver sensitivity of our system. Fig. 7(a-c) also shows BER vs. P_{RX} when the NOMA-CAP signal is simultaneously transmitted through the cores of the 2 km 7-core

MCF, providing a total transmission aggregated bit rate T_{R_b}= {350, 490, 630} Gb/s for R_b= {50, 70, 90} Gb/s per spatial channel, respectively. The BER curves for each core have been measured as the averaged among all bands of the transmitted NOMA-CAP signal when the power ratio between the two NOMA levels has been fixed to the optimized value of 7 dB. Finally, negligible penalty is measured in the receiver sensitivity over 2 km fiber transmission compared to the B2B case due to the high resilience of multi-CAP to the chromatic dispersion [17].

Table 1. Summary of Back-to-back Sensitivities of the Strong and Weak NOMA Levels for Different Aggregated Bit Rates (R_b) when the Power Ratio is Fixed to 7 dB as well as the BER of each multi-CAP band at the Considered FEC Limit of 7% OH HD-FEC.

NOMA level	Parameter									
	R_b (Gb/s)	Sensitivity (dBm)	BER per each multi-CAP band (×E-4)							
			1	2	3	4	5	6	7	8	9
Strong	50	-10.1	4.0	4.1	4.3	4.7	4.9				
	70	-8.1	1.2	1.3	1.7	1.8	2.0	6.5	7.5		
	90	-4.2	0.9	1.1	1.3	1.4	1.6	2.9	3.5	3.9	5.4
Weak	50	-7.9	3.7	4.1	4.2	4.8	5.2				
	70	-5.9	1.1	1.2	1.8	2.3	2.6	5.9	7.1		
	90	-1.2	1.2	1.3	1.3	1.6	1.9	2.5	2.8	3.5	5.9

4. CONCLUSION

We have presented a novel solution to leverage the features of split-cables and H-cables, enabling advanced network topologies in data centers containing HPC islands for artificial intelligence. The solution comprises the exploitation of space division multiplexing through multi-core fibers and NOMA-CAP as a means to double the link capacity while maintaining easy demultiplexing of the tributary signals. To validate our proposal, firstly an experimental measurement in a DD system with a PIN-based receiver at different bit rates in a back-to-back configuration of two NOMA levels and different number of 2.5 GHz multi-CAP bands has been done. This first demonstration provides aggregated system capacities from 50 Gb/s to 90 Gb/s with sensitivities, for the strong NOMA level, in the range of -10.1 dBm (at 50 Gb/s) to -4.2 dBm (at 90 Gb/s) and, for the weak NOMA level, of -7.9 (at 50 Gb/s) dBm to -1.2 dBm (at 90 Gb/s). Finally, the transmission of NOMA-CAP signals through 2 km of 7-core MCF, providing different total aggregated traffics ranging from 350 Gb/s to 630 Gb/s, has been also demonstrated with negligible transmission penalty due to the strong resilience of multi-CAP to chromatic dispersion. These results push NOMA-CAP forward as a strong candidate for future optical interconnects that requiring split links, high capacity, high granularity and scalability. As a next research stage, optimization of the multi-CAP frequency band size, bit loading and modulation order optimization to increase the aggregated bandwidth through artificial intelligence optimization processes can be conducted; we expect substantial gains when optimization processes combine the particular transfer function of the components with the different variables within the NOMA-CAP modulation format. Current developments in PIC circuits, particularly in silicon photonics, where operational bandwidths for modulators and photodiodes are slowly reaching 40-50 GHz, may suggest that the concepts proposed and experimentally validated in this work may be suitable candidates to support Terabit communications in future optical interconnects.

ACKNOWLEDGEMENTS

This work was supported in part by ALLIANCE (TEC2017-90034-C2-2-R) project co-funded by FEDER, the European Union's Horizon 2020 research and innovation programme under grant agreement n^{o} 780997 (plaCMOS), as well as MINECO FPI-BES-2015-074302.

REFERENCES

1. J. J. V. Olmos et al., "400G Interconnects for Data Centres and High-Performance Computing–What is Next?," in Int. Conf. Transparent Opt. Netw., Bucharest, Rumania, 2018.
2. A. J. Strojwas, K. Doong and D. Ciplickas, "Yield and Reliability Challenges at 7nm and Below," in Electron Devices Technol. and Manufacturing Conf., Singapore, 2019.
3. S. Gupta et al., "7-nm FinFET CMOS Design Enabled by Stress Engineering Using Si, Ge, and Sn," IEEE Trans. Electron Devices, vol. 61, no. 5, pp. 1222-1230, 2014.
4. W. Bogaerts, "Scaling up silicon photonics: where are the challenges," in Opt. S. Workshop, Laussanne, Switzerland, 2017.
5. N. Stojanovic, C. Prodaniuc, L. Zhang and J. Wei, "210/225 Gbit/s PAM-6 Transmission with BER Below KP4-FEC/EFEC and at Least 14 dB Link Budget," in European Conference on Optical Communication (ECOC), Rome, 2018.
6. A. Masuda, et al., "96-Gbaud PAM-4 Transmission with 1 sample/symbol under 22-GHz Bandwidth Limitation Using NL-MLSE Based on Third-Order Volterra Filter," in European Conference on Optical Communication (ECOC), Rome, Italy, 2018.
7. J. M. Estaran et al., "Sub-Baudrate Sampling at DAC and ADC: Toward 200G per Lane IM/DD Systems," IEEE J. of Lightw. Technol., vol. 37, no. 6, pp. 1536-1542, 2019.
8. N. Stojanovic et al., "4D PAM-7 Trellis Coded Modulation for Data Centers," IEEE Photonics Technol. Lett., vol. 31, no. 5, pp. 369-372, 2019.
9. Q. Hu et al., "Up to 94 GBd THP PAM-4 Transmission with 33 GHz Bandwidth Limitation," in European Conference on Optical Communication (ECOC), Rome, 2018.
10. F. Zhang *et al*., "Up to Single Lane 200G Optical Interconnects with Silicon Photonic Modulator," *in Optical Fiber Communications Conference and Exhibition (OFC)*, San Diego, 2019.
11. T. Wettlin et al., "Beyond 200 Gb/s PAM4 Transmission using Tomlinson-Harashima Precoding," in European Conference on Optical Communication (ECOC), Dublin, 2019.
12. Q. Hu et al., "High Data Rate Tomlinson-Harashima Precoding-based PAM Transmission," in European Conference on Optical Communication (ECOC), Dublin, 2019.
13. Q. Hu et al., "84 GBd Faster-Than-Nyquist PAM-4 Transmission using Only Linear Equalizer at Receiver," in Optical Fiber Communications Conference and Exhibition (OFC), San Diego, 2019.
14. K. Zhong et al., "Experimental study of PAM-4, CAP-16, and DMT for 100 Gb/s Short Reach Optical Transmission Systems," Opt. Express, vol. 23, pp. 1176-1189, 2015.
15. J. Wei et al., "Performance and Power Dissipation Comparisons Between 28 Gb/s NRZ, PAM, CAP and Optical OFDM Systems for Data Communication Applications," IEEE J. Lightw. Technol., vol. 30, no. 20, pp. 3273-3280, 2012.

16. D. Zou, Z. Li, Y. Sun, . Li, and Z. Li, “Computational complexity comparison of single-carrier DMT and conventional DMT in data center interconnect,” Opt. Express. vol. 27, pp. 17007-17016, 2019.
17. M. I. Olmedo et al., “Multiband carrierless amplitude phase modulation for high capacity optical data links,” IEEE J. Lightw. Technol., vol. 32, no. 4, pp. 798-804, 2014.
18. K. Kakizaki and S. Sasaki, “120-Gbit/s/pol./λ IM-DD Transmission over 55-km SSMF with 10-GHz-Bandwidth Intensity Modulator, Single PD, and a Pair of DAC and ADC with 20 GSa/s,” Optical Fiber Communications Conference and Exhibition (OFC), San Diego, 2019.
19. D. Zou et al., “Comparison of null-subcarriers reservation and adaptive notch filter for narrowband interference cancellation in intra-data center interconnect with DMT signal transmission”, Opt. Express, vol. 27, pp. 5696-5702, 2019.
20. J. Wei et al., “56 Gb/s multi-band CAP for data center interconnects up to an 80 km SMF,” Opt. Lett., vol. 41, pp. 4122-4125, 2016.
21. G. Im, D. B. Harman, G. Huang, A. V. Mandzik, M. Nguyen and J. Werner, “51.84 Mb/s 16-CAP ATM LAN standard,” IEEE J. Sel. Areas Commun., vol. 13, no. 4, pp. 620-632, 1995.
22. J. L. Wei, C. Sanchez, and E. Giacoumidis, “Fair comparison of complexity between a multi-band CAP and DMT for data center interconnects,” Opt. Lett., vol. 42, pp. 3860-3863, 2017.
23. G. Son et al., “High-efficiency broadband light coupling between optical fibers and photonic integrated circuits,” J. Nanophotonics, vol. 7, no 12, pp. 1845-1864, 2018.
24. Rosendo, Daniel, et al. “A methodology to assess the availability of next-generation data centers,” J. Supercomputing, pp. 1-25, 2019.
25. Infinera, “Rise of high-capacity data center interconnect in hyper-scale service provider systems,” [Online]. Available: https://www.infinera.com/
26. X. Chen et al., “Multimode and single-mode transmission over universal fiber for data center applications,” Optical Fiber Technology, vol. 44, pp. 53-60, 2018.
27. O. Ozolins et al., “7×149 Gbit/s PAM4 Transmission over 1 km Multicore Fiber for Short-Reach Optical Interconnects,” in Conf. on Lasers and Electro-Optics (CLEO), San Jose, 2018.
28. R. Lin et al., “Real-time 100 Gbps/λ/core NRZ and EDB IM/DD transmission over multicore fiber for intra-datacenter communication networks,” Opt. Express, vol. 26, pp. 10519-10526, 2018.
29. J. Van Kerrebrouck et al., “High-Speed PAM4-Based Optical SDM Interconnects With Directly Modulated Long-Wavelength VCSEL,” IEEE J. of Lightw. Technol., vol. 37, no. 2, pp. 356-362, 2019.
30. M. Becker et al., “Single-Mode Multicore Fibers with Integrated Bragg Filters,” IEEE J. Lightw. Technol., vol. 34, no. 19, pp. 4572-4578, 2016.
31. Higuchi, Kenichi, and Anass Benjebbour, “Non-orthogonal multiple access (NOMA) with successive interference cancellation for future radio access,” IEICE Trans. Commun., vol. 98, no 3, pp. 403-414, 2015.
32. J. A. Altabas et al., “Nonorthogonal Multiple Access and Carrierless Amplitude Phase Modulation for Flexible Multiuser Provisioning in 5G Mobile Networks,” IEEE J. Lightw. Technol., vol. 35, no. 24, pp. 5456-5463, 2017.

33. V. Veeravalli and A. Mantravadi, “The coding-spreading tradeoff in CDMA systems,” IEEE J. Sel. Areas Comm., vol. 20, no. 2, pp. 396–408, 2002.
34. M. Al-Imari, P. Xiao, M. A. Imran and R. Tafazolli, “Uplink nonorthogonal multiple access for 5G wireless networks,” in Proc. of Inter. Symp. Wireless Comm. Syst., Barcelona, 2014, pp. 781-785.
35. L. Dai, et al., “Non-orthogonal multiple access for 5G: solutions, challenges, opportunities, and future research trends,” IEEE Comm. Mag., vol. 53, no. 9, pp. 74-81, 2015.
36. Samael Sarmiento, et al., “Optical Power Budget Enhancement in 50 Gb/s IM-DD PONs with NOMA-CAP Modulation and SOA-based Amplification,” in Int. Conf. Transparent Opt. Netw., Angers, France, 2019.
37. S. Sarmiento, et al., “Experimental Investigation of 50-90 Gb/s IM-DD NOMA-CAP Modulation for Short Range Optical Transmission Applications,” in OptoElectronics and Commun. Conf./Int. Conf. Photonics in Switching and Computing, Fukuoka, Japan, 2019.
38. S. Sarmiento, et al., “Split-enabled 490 Gb/s Optical Interconnect with Direct Detection NOMA-CAP and 7-Core Multi-Core Fibre,” in European Conf. Opt. Commun., Dublin, Ireland, 2019.
39. A. J. Zilkie et al., “Multi-Micron Silicon Photonics Platform for Highly Manufacturable and Versatile Photonic Integrated Circuits,” IEEE J. Selected Topics in Quantum Electronics, vol. 25, no. 5, pp. 1-13, 2019.
40. M. He, et al., “High-performance hybrid silicon and lithium niobate Mach–Zehnder modulators for 100 Gbit/s and beyond,” Nature Photonics, vol. 13, no 5, pp. 359-364, 2019.
41. W. Klaus et al., “Free-Space Coupling Optics for Multicore Fibers,” IEEE Photonics Technology Letters, vol. 24, no. 21, pp. 1902-1905, 2012.
42. Y. Mao, et al., “Real-time investigation of CAP transceivers with hybrid digital equalization for visible light communication,” Opt. Express, vol 27, no 7, pp. 9382-9393, 2019.
43. D. Bykhovsky and S. Arnon “OFDM Allocation Optimization for Crosstalk Mitigation in Multiple Free-Space Optical Interconnection Links,” IEEE J. Lightw. Technol., vol. 33, no. 13, pp. 2777-2783, 2015.
44. M. Rahman and H. Yanikomeroglu, “Enhancing cell-edge performance: A downlink dynamic interference avoidance scheme with inter-cell coordination,” IEEE Trans. Wireless Commun., vol. 9, no. 4, pp. 1414-1425, 2010.
45. J. Grubor and K. D. Langer, “Efficient signal processing in OFDM-based indoor optical wireless links,” J. Netw., vol. 5, no. 2, pp. 197-211, 2010.
46. B. Ghimire and H. Haas, “Self-organising interference coordination in optical wireless networks,” EURASIP J. Wireless Commun. Netw., vol. 2012, no. 1, 2012.
47. D. Bykhovsky and S. Arnon, “Multiple access resource allocation in visible light communication systems,” IEEE J. Lightw. Technol., vol. 32, no. 8, pp. 1594-1600, 2014.
48. Z. Dong, J. Yu and J. Lu, “Bandwidth-Efficient WDM-CAP-PON Using Digital Hilbert Single-Sideband Modulation,” IEEE Photonics Journal, vol. 7, no. 5, pp. 1-7, 2015.

49. J. Zhang et al., “11 × 5 × 9.3Gb/s WDM-CAP-PON based on optical single-side band multi-level multi-band carrier-less amplitude and phase modulation with direct detection,” Opt. Express, vol. 21, pp. 18842-18848, 2013.
50. J. Wei and E. Giacoumidis, "Multi-band CAP for Next-Generation Optical Access Networks Using 10-G Optics," in Journal of Lightwave Technology, vol. 36, no. 2, pp. 551-559, 15 Jan.15, 2018.
51. J. Wei et al., “100-Gb/s Hybrid Multiband CAP/QAM Signal Transmission Over a Single Wavelength,” IEEE *J. Lightw. Technol.,* vol. 33, no. 2, pp. 415-423, 2015.